ELSEVIER

Journal of Nuclear Materials 294 (2001) 160–167

journal of nuclear materials

www.elsevier.nl/locate/jnucmat

Molecular dynamics study of mixed oxide fuel

Ken Kurosaki [a,*], Kazuhiro Yamada [a], Masayoshi Uno [a], Shinsuke Yamanaka [a], Kazuya Yamamoto [b], Takashi Namekawa [b]

[a] *Department of Nuclear Engineering, Graduate School of Engineering, Osaka University, Yamadaoka 2-1, Suita, Osaka 565-0871, Japan*
[b] *Alpha-Gamma Section, Fuels and Materials Division, Irradiation Center, Oarai Engineering Center, Japan Nuclear Cycle Development Institute, Narita-cho 4002, Oarai–machi, Ibaraki 311-1393, Japan*

Abstract

In order to develop new techniques to calculate the physicochemical properties of MOX fuel, molecular dynamics methods were applied to UO_2, PUO_2, and $(U,Pu)O_2$. These methods enabled us to obtain the heat capacity and thermal conductivity from basic properties, viz., the lattice parameter, linear thermal expansion coefficient, and compressibility. Results for UO_2 showed both the existence of a Bredig transition and a peak in the heat capacity at high temperature. The lattice parameter, heat capacity, and thermal conductivity of MOX fuel were calculated from basic properties of UO_2 and PuO_2. These results showed that molecular dynamics techniques can be usefully applied to determine physicochemical properties of MOX fuel.

1. Introduction

Physicochemical properties of nuclear fuel are important to evaluate pellet–cladding interaction (PCI). However, there is limited information on these properties for uranium–plutonium mixed oxide (MOX) fuel, due to the difficulties associated with the high radiation fields. Because recycled fuel will be widely used in fast breeder reactors and/or transmutation reactors in the future, it is necessary to develop a new technique to evaluate the physicochemical properties of MOX fuel. Molecular dynamics (MD) calculations can be one useful technique, and provide information to understand the physicochemical properties of the fuel.

In recent years with the advance of computer simulation techniques, extensive MD studies [1–3] have been performed on UO_2 to understand its thermal properties. There are only a few studies of MD simulation for PuO_2 and $(U,Pu)O_2$ solid solutions. However, these studies were limited to a few properties, or a small temperature range. In the present study, MD calculations for UO_2, PuO_2, and $(U,Pu)O_2$ solid solution were performed to evaluate the physicochemical properties of MOX fuel.

2. Molecular dynamics calculation

The MD calculations for UO_2, PuO_2, and $(U_{0.8}Pu_{0.2})O_2$ were performed for a system of 324 ions (108 cations and 216 anions) initially arranged in a CaF_2 type crystal structure. The MD cell for UO_2 is shown in Fig. 1. In the present study, calculations were performed by a molecular dynamics program based on MXDRTO [4]. Standard constant pressure–temperature (NPT) and constant volume–temperature (NVT) MD calculations at thermodynamic equilibrium were performed. Quantum effects [5] were taken into account in the present calculation. In the $(U_{0.8}Pu_{0.2})O_2$ system, the desired number of plutonium ions were substituted randomly onto the uranium ion sites. The lattice, containing a fixed number of atoms, was assumed to repeat periodically throughout the material, and there was no edge or surface effect. Long-range coulomb interactions were treated with Ewald's summation [6]. The equations of motion were integrated using Verlet's algorithm [7] with an integration time step of 2.0×10^{-15} s. At the start of

* Corresponding author. Tel.: +81-6 6879 7905; fax: +81-6 6879 7889.
E-mail address: kurosaki@nucl.eng.osaka-u.ac.jp (K. Kurosaki).

0022-3115/01/$ - see front matter
PII: S0022-3115(01)00451-2

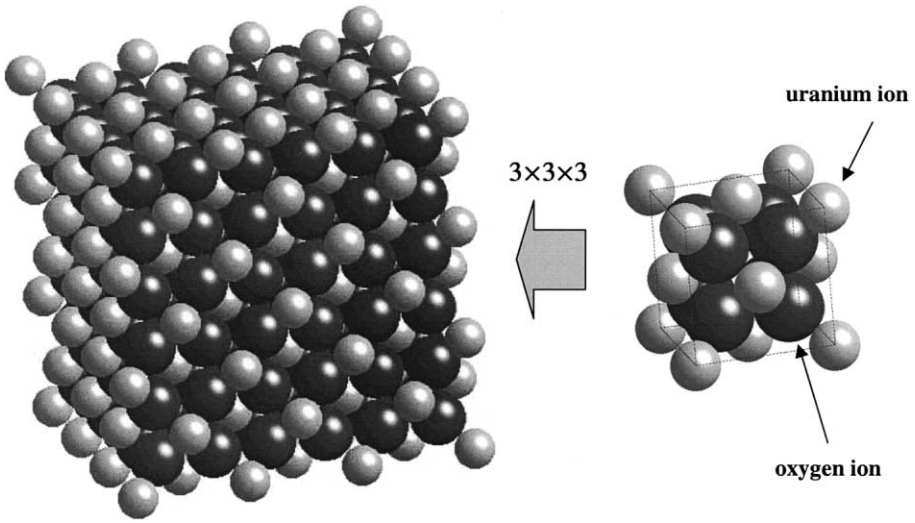

Fig. 1. MD cells for UO_2.

the calculation, the initial velocity of each atom was assumed to take random velocities, which was about 0.01 Å fs^{-1}.

The calculations were made in the temperature range from 300 to 2500 K, and in the pressure range from 0.1 MPa to 1.5 GPa. The temperature and pressure of the system were controlled independently through a simple velocity scaling. However, in calculating the thermal conductivities, a combination of the methods introduced by Andersen [8] and Nose [9] were used to control the pressure and temperature. A 10 000-step equilibrium run was made at the desired temperature and pressure. Although the number of steps was small, equilibrium was achieved as judged from the changes in the temperature (±3%), pressure (±9%), density (±0.02%) and internal energy (±0.04%). At 300 K, the mean square displacement of oxygen ions in the MD cell was within 0.02 Å^2, which is close to the magnitude of thermal vibrations at that temperature.

We employed the semi-empirical 2-body potential function proposed by Ida [10] for cation–anion interactions. In this potential, the f-electrons and relativistic effects are accounted for implicitly, but the 3-body effect is not accounted for. It would be desirable to use the 3-body (or beyond) potential. For the present study, however, the 2-body potential is sufficient though, because the system (fluorite structure) is relatively simple. The potential is a partially ionic model including a covalent contribution:

$$U_{ij}(r_{ij}) = \frac{z_i z_j e^2}{r_{ij}} + f_0(b_i + b_j)\exp\left(\frac{a_i + a_j - r_{ij}}{b_i + b_j}\right) - \frac{c_i c_j}{r_{ij}^6} + D_{ij}\{\exp\left[-2\beta_{ij}(r_{ij} - r_{ij}^*)\right] - 2\exp[-\beta_{ij}\left(r_{ij} - r_{ij}^*\right),$$

where f_0 equals 4.186, Z_i and Z_j are the effective partial electronic charges on the ith and jth ions, r is the atom distance, r_{ij}^* is the bond length of the cation–anion pair in vacuum, and a, b, and c are characteristic parameters depending on the ion species. In this potential function, D_{ij} and β_{ij} describe the depth and shape of this potential, respectively. The first term is the coulomb interaction, the second term denotes the core repulsion, and the third term, which is called Morse-type [11] potential, corresponds to the covalent contribution.

The parameters (a, b, c) for oxygen ions given by Kawamura [12] were used in the present study. These parameters have been used in the studies of other oxides such as $SiO_2, MgSiO_4, Al_2O_3$, and $NaAlSiO_4$ [12]. The other parameters were determined by trial and error using the experimental values of the changes in the lattice parameters with temperature and pressure for UO_2, PuO_2, and $(U_{0.8}Pu_{0.2})O_2$. This semi-empirical approach to determine the potential parameters has given effective and realistic results for crystalline solids [4], and MD studies using the same method are published [13–15]. Using the parameters so obtained, the linear thermal expansion coefficient (α), compressibility (β), heat capacity, and thermal conductivity of UO_2, PuO_2, and $(U_{0.8}Pu_{0.2})O_2$ were evaluated.

The thermal conductivity of the system was calculated by the Green–Kubo relations. Because the Green–Kubo theory is a statistical method, the NPT calculation was performed using the methods introduced by Andersen [8] and Nose [9]. Details of the Green–Kubo relations have been described in several other papers [16], so only the main points will be briefly described here.

The form of the thermal conductivity of the system is based on the integrated heat flux [$S(t)$] autocorrelation function:

$$\lambda = \frac{V}{3k_B T^2} \int_0^\infty \langle S(t) \cdot S(0) \rangle \mathrm{d}t,$$

where λ is the thermal conductivity, V is the volume of the system, T is the absolute temperature, and k_B is the Boltzmann constant. The heat flux S is described as

$$S = \frac{1}{V}\left[\sum_j e_j v_j - \frac{1}{2}\sum_j \sum_{j=i} r_{ij}(f_{ij} v_j)\right],$$

and the instantaneous excess energy of atom j, e_j, is described as

$$e_j = \left\{\frac{1}{2} m_j v_j^2 + \frac{1}{2}\sum_{i=j} u(r_{ij})\right\} - e_{av},$$

where m_j and v_j are the mass and velocity of atom j, and r_{ij}, f_{ij}, and u are the interatomic distance, force, and potential between atom i and j. The autocorrelation function was calculated for 5×10^5 steps with time origins taken at every 10 steps.

3. Results and discussion

3.1. Interatomic potential

The values of the parameters used in the interatomic potential in the present study are summarized in Table 1. The change in the lattice parameters of UO_2, PuO_2, and $(U_{0.8}Pu_{0.2})O_2$ with temperature obtained by the MD calculations, for 0.1 MPa are shown in Fig. 2, together with the experimental data [17,18]. The variation with temperature in the calculated lattice parameter agrees well with the reported values. For $(U_{0.8}Pu_{0.2})O_2$, it was found that the calculated lattice parameter followed Vegard's law up to high temperatures. Since various effects at high temperatures, such as formation of Frenkel defects, are not taken into account in the present calculations, the deviation of the calculated values from the experimental values appears to increase with increasing temperature. The change in the lattice parameter of UO_2 with pressure in the range from 0.1 MPa to 1.5 GPa at 300 K was also studied, and these results are in agreement with the experimental values [19,20]. These results indicate that the potential function used in the present calculations describes well the changes in the lattice parameter with both temperature and pressure.

3.2. Thermal expansion and compressibility

Linear thermal expansion coefficients (α) of UO_2, PuO_2, and $(U_{0.8}Pu_{0.2})O_2$ can be obtained from the change of the lattice parameters with temperature. Although the calculated values of α were slightly lower (about 5%) than the experimental data [17,18], the tendency of the temperature dependence was consistent with the experimental data.

The compressibility (β) at pressures from 0.1 MPa to 1.5 GPa was evaluated up to about 2500 K from the change in lattice parameter with pressure. The temperature dependence of the calculated β for UO_2, PuO_2, and $(U_{0.8}Pu_{0.2})O_2$, together with the experimental data [19,20] are shown in Fig. 3. For UO_2, the calculated β is in good agreement with the experimental data, increasing with increasing temperature in a similar manner to the experimental data. This means that the MD cell of UO_2 becomes mechanically soft with increasing temperature. At high temperatures, the calculated β increased markedly. It is known that UO_2 becomes soft and the creep rate of UO_2 increases at high temperatures. This phenomenon was well reproduced by the MD simulation. The β of stoichiometric PuO_2 has not been reported until now. It increases with increasing temperature. The marked increase of the calculated β at high temperatures was not observed for PuO_2. For $(U_{0.8}Pu_{0.2})O_2$, the calculated β (5.5×10^{-3} GPa) is slightly lower than the literature data [20] (6.3×10^{-3} GPa) at room temperature, which is caused by the difference in the structures between the MD cell (a perfect single crystal) and the experimental specimen (polycrystalline). The calculated β of $(U_{0.8}Pu_{0.2})O_2$ increased markedly at high temperatures as did UO_2.

Jackson [21] has showed that cation migration is assisted by anion diffuse transition (Bredig transition). The Bredig transition may occur at high temperatures in the MD cells of UO_2 and $(U_{0.8}Pu_{0.2})O_2$, and this would generate the marked increases of the calculated βs. This will be confirmed in Section 3.4.

Table 1
Values of the interatomic potential function parameters

Ions	z	a	b	c	D_{ij}	β_{ij}	r^*_{ij}
O	−1.2	1.926	0.160	20			
					(for U–O pairs)		
U	2.4	1.659	0.160	0	18.0	1.25	2.369
					(for Pu–O pairs)		
Pu	2.4	1.229	0.080	0	13.0	1.56	2.339

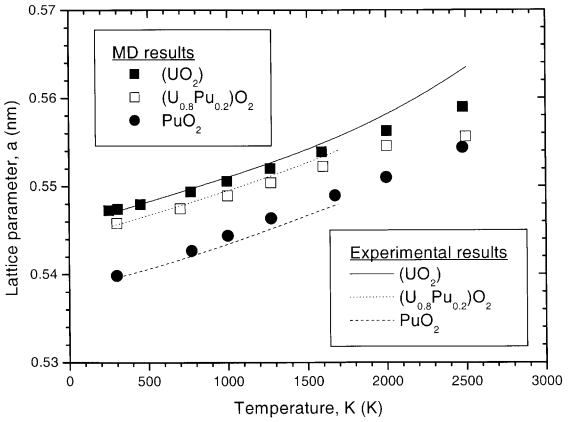

Fig. 2. Calculated lattice parameters for UO_2, PuO_2, and $(U_{0.8}Pu_{0.2})O_2$ as a function of temperature.

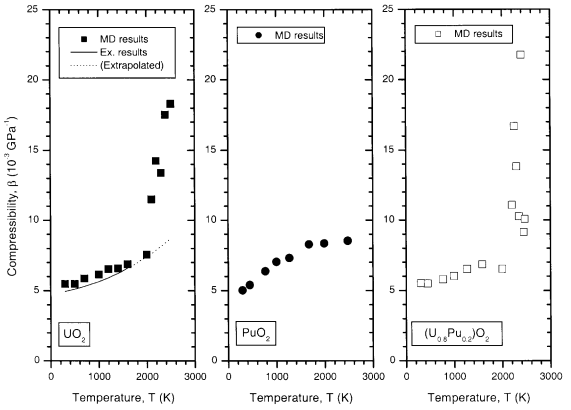

Fig. 3. Calculated compressibility (β) for UO_2, PuO_2, and $(U_{0.8}Pu_{0.2})O_2$ as a function of temperature.

3.3. Heat capacity

By using the same parameters for the interatomic potential that were determined from the lattice parameter variations, the heat capacities of UO_2, PuO_2, and $(U_{0.8}Pu_{0.2})O_2$ were evaluated. The heat capacity at constant pressure C_P can be evaluated approximately from the following relationship:

$$C_P = C_V + C_d + C_{el} + C_{sch} + C_{sp} + \cdots,$$

where C_V is the heat capacity at constant volume, C_d is the lattice dilational term, C_{el} is the conduction electronic term, C_{sch} is the Schottky term, and C_{sp} is the contribution from the formation of the small polarons. We evaluated C_P for the three materials as follows:

$$C_P(UO_2) = C_V(MD) + C_d(MD) + C_{sch}(UO_2) + C_{sp}(UO_2),$$

$$C_P(PuO_2) = C_V(MD) + C_d(MD) + C_{sch}(PuO_2) + C_{sp}(UO_2),$$

$$C_P((U_{0.8}Pu_{0.2})O_2) = C_V(MD) + C_d(MD) + 0.8(C_{sch}(UO_2) + C_{sp}(UO_2)) + 0.2C_{sch}(PuO_2).$$

Only C_V and C_d can be evaluated using the results obtained from the MD calculations. C_{sch} (Schottky term) and C_{sp} (small polarons term) are taken from the literature [22,23]. The conduction electron contribution is ignored, since UO_2, PuO_2, and $(U_{0.8}Pu_{0.2})O_2$ are considered to behave like insulators.

In the present study, C_V was evaluated from the variation of the internal energy of the system with temperature calculated by the NVT MD simulations. C_d was evaluated from the following relationship:

$$C_d = \frac{(3\alpha)^2 VT}{\beta},$$

where V is the molar volume, α is the linear thermal expansion coefficient, β is the compressibility, and T is the absolute temperature. C_d was evaluated by using the calculated values of α, V, and β obtained from the NPT MD simulations. Since the contributions of the conduction electrons, the Schottky defects, and the formation of the small polarons were not simulated in the present calculation, literature data [22] were used. For UO_2, the Schottky contribution to the internal energy (U) is given by

$$U_{sch} = 1.46 \cdot t^2 \ (\text{kJ mol}^{-1}),$$

where $t = 10^{-3}\ T$ (K), and the contribution from the formation of the small polarons ($2U^{4+} \rightarrow U^{3+} + U^{5+}$) to the internal energy (U) is given by

$$U_{sp} = 256 \exp\left(\frac{-10.79}{t}\right) \quad \text{kJ mol}^{-1}.$$

In the present study, each contribution to the heat capacity was obtained from a differentiation of the internal energy by temperature.

The change in the calculated C_P with temperature for UO_2 is shown in Fig. 4, together with the literature data [24–26]. In the temperature range from 300 to 2500 K, the calculated C_P agrees well with both MALT-2 [25] and SGTE [26] data, which indicates that the potential function used in the present study describes well the change in the internal energy of UO_2 with temperature.

For PuO_2, C_P was calculated by adding C_d, C_{sch}, and C_{sp} (for UO_2) to C_V. C_V was calculated from the variation of the internal energy of the system with temperature by the NVT simulations, similar to the case of UO_2. The Schottky contribution to the heat capacity for PuO_2 has been reported by Manes [23]. It is known that C_P for PuO_2 is higher than that for UO_2. The main reason

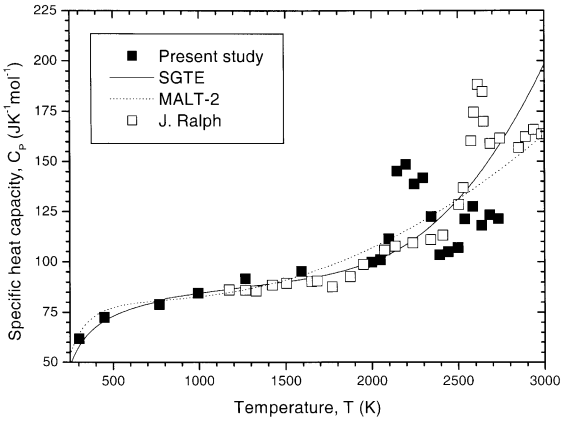

Fig. 4. Temperature dependence of C_P for UO_2.

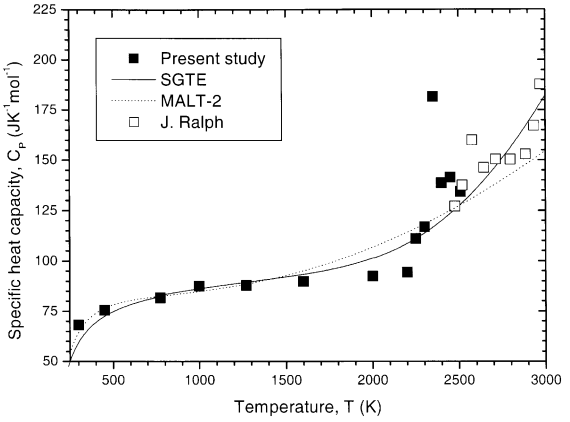

Fig. 6. Temperature dependence of C_P for $(U_{0.8}Pu_{0.2})O_2$.

is that the Schottky contribution of PuO_2 to the heat capacity is larger than that for UO_2. Fig. 5 shows the variation in the calculated C_P for PuO_2 with temperature, together with the literature data [24–26]. Fig. 5 shows the poor agreement between the calculated C_P and that measured by Ralph [24]. The reason for the poor agreement is not understood yet. However, the calculated result is considered to be reasonable, because the agreement with other data (SGTE and MALT-2) can be observed in the figure.

For $(U_{0.8}Pu_{0.2})O_2$, C_P was obtained by adding C_d, C_{sch}, and C_{sp} to C_V. Eighty percent of the values of C_{sch} and C_{sp} for UO_2 and 20% of the values of C_{sch} for PuO_2 were used. Fig. 6 shows the results, together with the literature data [24–26]. It is observed that the results agree with the Neumann–Kopp's law. At about 2350 K, the calculated C_P shows a peak as already seen for UO_2, which indicates the occurrence of a Bredig transition in the simulated MD cells.

3.4. Bredig transition

It has been reported [27] that a diffuse transition (Bredig transition) occurs at about 0.8 of the melting temperatures in many fluorite structure compounds $(SrCl_2, PbF_2, ThO_2, UO_2)$. The Bredig transition is characterized by a smooth peak in the heat capacity [28], a dramatic rise in the electrical conductivity [29], and a rapid increase in disorder of the anion sublattice [30]. In the present study, the Bredig transition can be observed in the calculated C_V for UO_2 and 20%-MOX but not for PuO_2. For example, the calculated C_V for UO_2 is shown in Fig. 7 as a function of temperature. The Bredig transition is observed in C_V, independently of the Schottky and other effects, which means that the Bredig transition can be reproduced by the potential effects.

The motion tracks of some ions for UO_2 and PuO_2 unit cells at 2500 K are shown in Fig. 8. The large motion of oxygen ions is observed in the figure, and it is

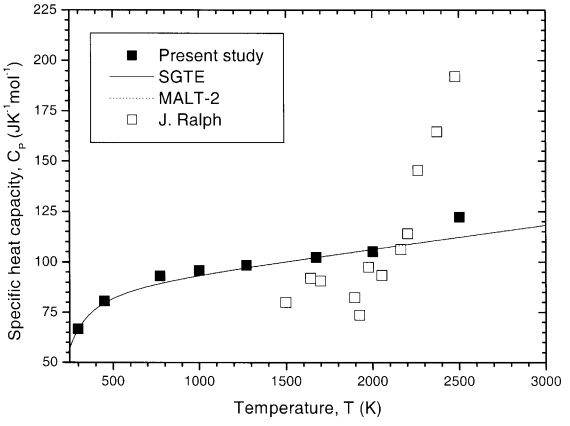

Fig. 5. Temperature dependence of C_P for PuO_2.

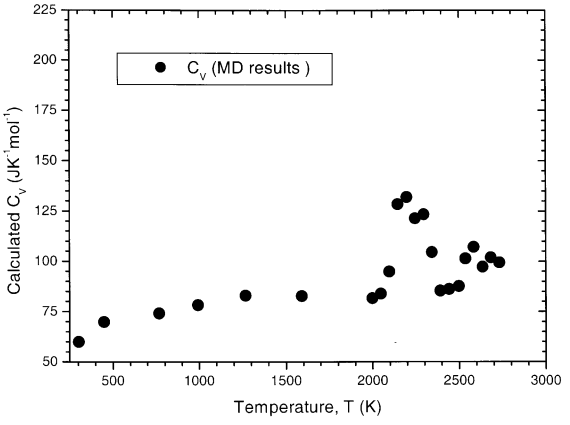

Fig. 7. Calculated C_V for UO_2 as a function of temperature.

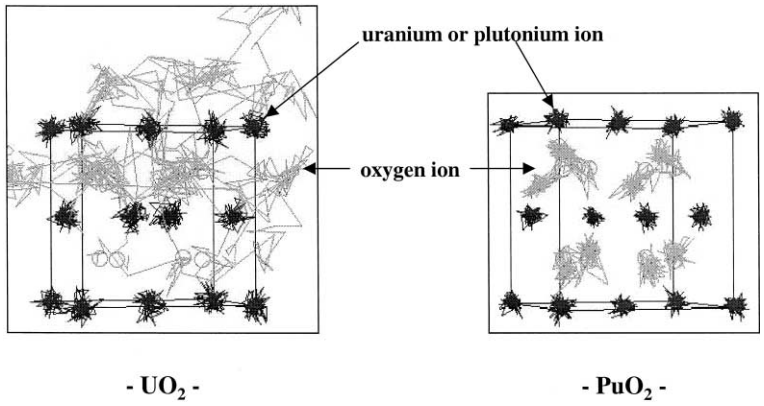

Fig. 8. Motion tracks of ions for UO_2 and PuO_2 unit cells at 2500 K.

suggested that the MD cell of UO_2 becomes an oxygen superionic conductor at the temperature as confirmed by neutron scattering experiments [31]. Ralph [24] has reported that a Bredig transition of UO_2 occurs at 2610 K (0.84 of the melting temperature), which is almost in agreement with the present calculation. This result provides further confirmation that our model can give a reasonable description of the atomic motion in UO_2 at high temperatures.

Clear existence of a Bredig transition in PuO_2 has not been reported. Ralph [24] concluded that it might occur in PuO_2, although his enthalpy data analysis did not detect a heat capacity peak for PuO_2. He pointed out that insufficient data in the vicinity of 0.8 of the absolute melting temperature may have been the reason. In the present calculation, the Bredig transition did not occur in the simulated PuO_2 MD cell even at 2500 K (0.94 of the melting temperature). Therefore, it is concluded that the transition temperature might be very near to the melting temperature for PuO_2.

3.5. Thermal conductivity

The thermal conductivity of UO_2, PuO_2, and $(U_{0.8}Pu_{0.2})O_2$ were evaluated by the MD calculation. Only lattice contributions to the thermal conductivity, λ_{lat} could be included in the calculations. The λ_{lat} was obtained as the plateau value of the time integral of the auto-correlation function (ACF) of energy current, $\langle S(t)S(0)\rangle$. The ACF approaches zero and its time integral reaches a plateau value. Integrating ACF with respect to time gives the thermal conductivity. Details of these calculations are given in our previous papers [32–35].

For UO_2, the variation in calculated thermal conductivity with temperature is shown in Fig. 9, together with the literature data [36]. The high temperature electronic contribution to thermal conductivity, predicted by Harding [37], was added to the calculated value at 2000 and 2500 K. The result is in good agreement with the experimental values in the temperature range from 650 to 2500 K, even though the simulated system is a perfect crystal. This indicates that our model can describe the phonon contribution to the thermal conductivity.

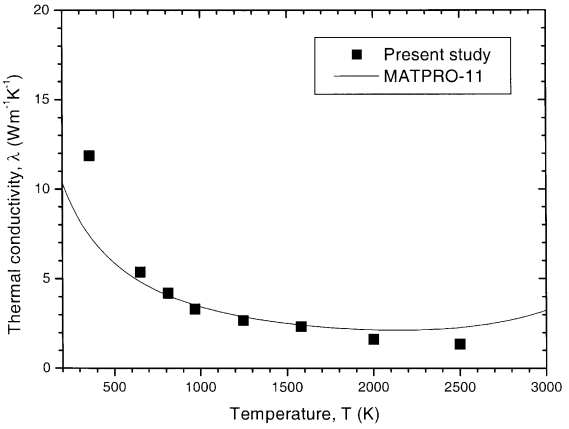

Fig. 9. Temperature dependence of thermal conductivity for UO_2.

The calculated thermal conductivity of PuO_2 is shown in Fig. 10 as a function of temperature, together with the experimental data reported by Gibby [38]. The calculated values are in good agreement with the experimental data in the temperature range from 360 to 2000 K, showing that the simulated system of PuO_2 models the phonon vibration well. This provides further confirmation that the potential model of PuO_2 in the present study is reasonable for computing the thermal conductivity.

The calculated thermal conductivity of $(U_{0.8}Pu_{0.2})O_2$ is shown in Fig. 11 as a function of temperature, together with the literature data [38–44]. 80% of the

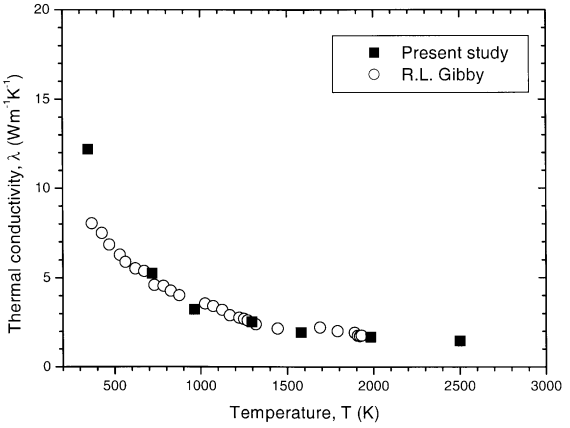

Fig. 10. Temperature dependence of thermal conductivity for PuO_2.

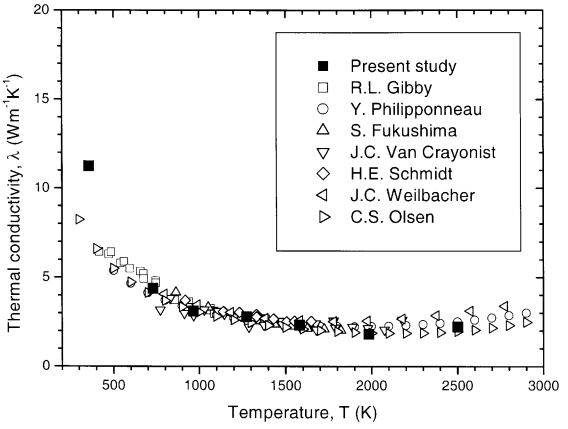

Fig. 11. Temperature dependence of thermal conductivity for $(U_{0.8}Pu_{0.2})O_2$.

electronic contribution in UO_2 predicted by Harding [37] was added to the calculated values at 2000 and 2500 K. The result is in good agreement with the experimental values up to 2500 K, and is lower than that of both UO_2 and PuO_2. This indicates that plutonium ions act as the phonon scattering centers in the MD cell, similar to the real materials.

4. Summary

MD calculations were performed for UO_2, PuO_2, and $(U_{0.8}Pu_{0.2})O_2$ to evaluate the physicochemical properties. The simulated UO_2 system showed both the existence of the Bredig transition and a peak in the heat capacity at high temperatures, and provided thermal conductivities in the temperature range from 360 to 2500 K. The variation in the calculated heat capacity of PuO_2 with temperature agreed well with the experimental data. The change in the calculated thermal conductivity of PuO_2 with temperature was also in good agreement with the experimental data. This indicated that the simulation model of PuO_2 gave a reasonable description of the phonon contribution to the thermal conductivity. The Bredig transition did not occur in the simulated PuO_2 system. The lattice parameter, compressibility, heat capacity, and thermal conductivity of $(U_{0.8}Pu_{0.2})O_2$ were also evaluated from some basic properties of UO_2 and PuO_2 by using the molecular dynamics techniques. The calculated lattice parameter of $(U_{0.8}Pu_{0.2})O_2$ closely followed Vegard's law. The calculated heat capacity and thermal conductivity of $(U_{0.8}Pu_{0.2})O_2$ were in good agreement with the experimental data. The simulated $(U_{0.8}Pu_{0.2})O_2$ cell also showed both the existence of the Bredig transition and a peak in the heat capacity at about 2350 K.

These results showed the usefulness of the molecular dynamics techniques for evaluation of the physicochemical properties of the nuclear fuel. Molecular dynamics will become a powerful method to evaluate the thermal and mechanical properties of fuel with a multicomponent system.

References

[1] C.R.A. Catlow, Proc. R. Soc. A 353 (1977) 533.
[2] P.J.D Lindan, M.J. Gillan, J. Phys. Condens. Mater. 3 (1991) 3929.
[3] S. Higuchi, J. Nucl. Sci. Technol. 35 (1998) 833–835.
[4] K. Kawamura, K. Hirao, Material Design Using Personal Computer, Shokabo, Tokyo, 1994.
[5] E. Wigner, Phys. Rev. 40 (1932) 749.
[6] P.P. Ewald, Ann. Phys. 64 (1921) 253.
[7] L. Verlet, Phys. Rev. 159 (1967) 98.
[8] H.C. Andersen, J. Chem. Phys. 72 (1980) 2384.
[9] S. Nose, J. Chem. Phys. 81 (1984) 511.
[10] Y. Ida, Phys. Earth Planet Interiors 13 (1976) 97.
[11] P.M. Morse, Phys. Rev. 34 (1929) 57.
[12] K. Kawamura, Solid State Sci. 103 (1992) 88.
[13] T. Katsumata, Y. Inaguma, M. Itoh, K. Kawamura, Solid State Ionics 108 (1998) 175.
[14] H. Inaba, R. Sagawa, H. Hayashi, K. Kawamura, Solid State Ionics 122 (1999) 95.
[15] H. Hayashi, R. Sagawa, H. Inaba, K. Kawamura, Solid State Ionics 131 (2000) 281.
[16] R. Zwanzig, Ann. Rev. Phys. Chem. 16 (1965) 67.
[17] D.G. Martin, J. Nucl. Mater. 152 (1988) 94.
[18] Thermophysical properties of matter, The TPRC data series vol. 5, IFI/Plenum Data, New York, 1970.
[19] P. Browning, G.J. Hyland, J. Ralph, High Temp.-High Pressures 15 (1983) 169.
[20] A.W. Nutt, A.W. Allen, J. Am. Ceram. Soc. 53 (1970) 205.
[21] R.A. Jackson, A.D. Murray, J.H. Harding, C.R.A. Catlow, Philos. Mag. A 53 (1986) 27.
[22] G.J. Hyland, J. Ralph, High Temp.–High Pressures 15 (1983) 179.

[23] L. Manes, Plutonium 1970 and Other Actinides, Part 1, p. 254.
[24] J. Ralph, J. Chem. Soc., Faraday Trans. 2&83 (1987) 1253.
[25] Japan Thermal Measurement Society, Thermodynamics Data Base for Personal Computer MALT 2, 1992.
[26] The SGTE Pure Substance and Solution databases, GTT-DATA SERVICES.
[27] A.S. Dworkin, M.A. Bredig, J. Phys. Chem. 72 (1968) 1277.
[28] W. Schroter, J. Nolting, J. Phys. Colloq. (Paris) C 6 (41) (1980) 20.
[29] M.J. Gillan, UKAEA Harwell Report TP 1097.
[30] M.H. Dickens et al., J. Phys. C 15 (1982) 4043.
[31] K. Clausen, W. Hayes, J.E. Macdonald, R. Osborn, M.T. Hutchings, Phys. Rev. Lett. 52 (1984) 1238.
[32] K. Yamada, K. Kurosaki, M. Uno, S. Yamanaka, J. Alloys Compounds 307 (2000) 1.
[33] K. Yamada, K. Kurosaki, M. Uno, S. Yamanaka, J. Alloys Compounds 307 (2000) 10.
[34] K. Kurosaki, K. Yano, K. Yamada, M. Uno, S. Yamanaka, J. Alloys Compounds 311 (2000) 305.
[35] K. Kurosaki, K. Yano, K. Yamada, M. Uno, S. Yamanaka, J Alloys Compounds 313 (2000) 242.
[36] MATPRO-Version 11 (Revision 2), NUREG/CR-0497, TREE-1280, Rev. 2, August 1981.
[37] J.H. Harding, D.G. Martin, J. Nucl. Mater. 166 (1989) 233.
[38] R.L. Gibby, J. Nucl. Mater. 38 (1971) 163.
[39] Y. Philipponneau, J. Nucl. Mater. 188 (1992) 194.
[40] S. Fukushima, T. Ohmichi, A. Maeda, M. Handa, J. Nucl. Mater. 16 (1983) 287.
[41] J.C. Van Crayonist, J.C. Weilbacher, Rapport SYRIA-3488, 1968.
[42] H.E. Schmidt, High-Temp.-High-Pressures 3 (1971) 345.
[43] J.C. Weilbacher, Rapport SYRIA-4572, 1972.
[44] C.S. Olsen, G.A. Reymann, in: P.E. MacDonald, L.B. Thompson (Eds.), THREE-NUREG-1005, 1976.